QUIET-SUN NETWORK BRIGHT POINT PHENOMENA WITH SIGMOIDAL SIGNATURES

The Astrophysical Journal, 814:124 (10pp), 2015 December 1 doi:10.1088/0004-637X/814/2/124

QUIET-SUN NETWORK BRIGHT POINT PHENOMENA WITH SIGMOIDAL SIGNATURES

D. L. Chesny[1,2], H. M. Oluseyi[1,3], N. B. Orange[2], and P. R. Champey[4]
[1] Department of Physics & Space Sciences, Florida Institute of Technology, Melbourne, FL 32901, USA
[2] OrangeWave Innovative Science, LLC, Moncks Corner, SC 29461, USA
[3] Massachusetts Institute of Technology, Department of Physics, Cambridge, MA 02139, USA
[4] Department of Optical Science and Engineering, University of Alabama in Huntsville, Huntsville, AL 35899, USA
Received 2015 June 22; accepted 2015 September 22; published 2015 November 25

ABSTRACT

Ubiquitous solar atmospheric coronal and transition region bright points (BPs) are compact features overlying strong concentrations of magnetic flux. Here, we utilize high-cadence observations from the Atmospheric Imaging Assembly on board the *Solar Dynamics Observatory* to provide the first observations of extreme ultraviolet quiet-Sun (QS) network BP activity associated with sigmoidal structuring. To our knowledge, this previously unresolved fine structure has never been associated with such small-scale QS events. This QS event precedes a bi-directional jet in a compact, low-energy, and low-temperature environment, where evidence is found in support of the typical fan-spine magnetic field topology. As in active regions and micro-sigmoids, the sigmoidal arcade is likely formed via tether-cutting reconnection and precedes peak intensity enhancements and eruptive activity. Our QS BP sigmoid provides a new class of small-scale structuring exhibiting self-organized criticality that highlights a multi-scaled self-similarity between large-scale, high-temperature coronal fields and the small-scale, lower-temperature QS network. Finally, our QS BP sigmoid elevates arguments for coronal heating contributions from cooler atmospheric layers, as this class of structure may provide evidence favoring mass, energy, and helicity injections into the heliosphere.

Key words: magnetic reconnection – Sun: atmosphere – Sun: corona – Sun: magnetic fields

1. INTRODUCTION

Coronal and transition region (TR) X-ray and extreme ultraviolet (EUV) bright points (BPs; e.g., Shibata et al. 1992, 1996; Shimojo et al. 1996; Shimojo & Shibata 2000) that predominantly follow the bipole reconnection model as self-similar manifestations of large-scale active regions (ARs) are sources of jet phenomena that contribute directly to coronal heating and solar wind mass feeding (Kamio et al. 2011; Orange et al. 2014b; Tian et al. 2014). Although at some coronal heights and temperatures, individual BP loops have been resolved (Kankelborg et al. 1996), the spatial resolution of Sun-observing instruments have been insufficient to probe the formation and evolution of BPs due to the existence of unresolved fine structure (UFS) and the dynamics of the plasma and magnetic field environment (Zhang et al. 2012). Of distinct interest is that resolution of these fundamental qualities should provide insight into conditions leading to BP jet formation, heating mechanisms, and contributions to upward mass flux. Ultimately, these findings will inform the details of solar EUV variability, coronal heating, and solar wind mass sources.

BPs are stochastic brightenings that form along the polarity inversion lines (PILs) of strong photospheric magnetic bipole regions (Kankelborg et al. 1996; Longcope et al. 2001) and have been suggested to be small-scale, self-similar manifestations of ARs (Longcope et al. 2001; Orange et al. 2014b) due to their compact clustering of loops over distinct bipolar regions. One aspect missing from coronal and TR BP analyses is the ability to predict whether any individual configuration will exhibit eruptive behavior. AR dynamics leading to explosive activity and coronal mass ejections (CMEs) can sometimes be preceded by the appearance of sigmoids prior to the eruption (Canfield et al. 1999; Moore et al. 2001). Sigmoids are "S-shaped" loop arcades that originate at the magnetic footpoints of ARs. These non-potential fields signal the breakdown of magnetic stability and sometimes signal the oncoming opening of the overlying magnetic canopy, thereby allowing for the release of high-temperature plasma into interplanetary space. Studies highlighting BPs with sigmoidal structuring hold significant potential for work toward the development of predictability techniques of eruptive phenomena in this feature class.

Recently, a self-similar AR-coronal BP jet connection was made when Raouafi et al. (2010) observed micro-sigmoids at the bases of coronal jets in XRT data. The authors found that these micro-sigmoids were manifestations of merging "J-shaped" loops at scales significantly smaller than their AR counterparts (McKenzie & Canfield 2008). Such observations and dynamics, along with EUV observations of micro-sigmoids (Zheng et al. 2013), point to a possible multi-scaled self-similarity in the ensemble of sigmoid events leading to eruptive activity. Raouafi et al. (2010) concluded that if there are self-similarities between event properties and instability mechanisms, then the eruptions of micro-sigmoids could lead to magnetic energy dissipations and injections of helicity into the heliosphere.

Studies of the three-dimensional morphology of jet phenomena have unveiled connections between the photospheric magnetic field evolution and the dynamical atmospheric plasma response. Liu et al. (2011) studied an equatorial coronal hole (CH) chromospheric jet with *Hinode* SOT (Tsuneta et al. 2008) and found the first evidence for simultaneous emerging magnetic flux and resulting jet development. Evidence exists for such CH jet formation due to interchange reconnection between closed flux tubes and existing open fields (Krista et al. 2011). It is due to the reconnection of the emerging magnetic energy with the existing open field structure that induces a magnetic null point (NP), about which the spine axis releases a collimated stream of plasma into the upper atmosphere (Masson et al. 2012). This NP-jet formation

process has also been associated with mixed-polarity closed fields where the reconnection occurs above a separatrix dome and results in bi-directional current sheets (Pontin et al. 2013). These authors cite the ubiquity of NPs throughout the solar atmosphere for the importance of understanding the various photospheric field conditions that lead to jet activity. Tian et al. (2014) suggested that jet phenomena with propagation speeds of 80–250 km s^{-1} are intermittent but persistent sources of mass and energy to the corona and noted that they must be considered in any successful model of the TR or the heating of the solar wind.

To probe formation and instability mechanisms, attention must be given to the source magnetic field configurations of jet events. The previously considered events (except Raouafi et al. 2010) were associated directly with large-scale concentrations of bipolar magnetic flux. However, it is an open question as to whether the small-scale network magnetic flux of the quiet Sun (QS) can form and sustain EUV BP activity with sigmoidal structuring and dynamics self-similar to their higher temperature counterparts. The QS network is known to be able to sustain non-potential fields and sigmoidal activity (Chesny et al. 2013), but non-potentiality has only been associated with high-temperature BP activity by Raouafi et al. (2010). Evidence of such cool activity will show a multi-scaled self-similarity in the sigmoid–BP relationship down to the QS network scale.

This study utilizes observations from the Atmospheric Imaging Assembly (AIA; Lemen et al. 2012) and Heliospheric and Magnetic Imager (HMI; Schou et al. 2012) instruments on board the *Solar Dynamics Observatory* (Pesnell 2008) to analyze small-scale BP plasma and magnetic field structuring and dynamics that have not been resolved in previous observational data sets. These unique data may help to resolve whether certain instability mechanisms are self-similar throughout different temperature and magnetic field regimes in the solar atmosphere. Raouafi et al. (2010) noted that the spatial resolution of XRT observations is insufficient for resolving very small BPs, so we look to address the question as to whether there are QS-scale BPs that can be associated with sigmoid activity. These data may provide the observations of unique simultaneous magnetic field dynamics and jet development in the QS. Here, for the first time, sigmoidal structuring has been observed accompanying eruptive BP phenomena in the EUV QS network.

2. OBSERVATIONS AND DATA REDUCTION AND ENHANCEMENT

AIA is a narrow passband imager containing four telescopes sequentially observing seven EUV and two FUV bands[5] at 0.″6 $pixel^{-1}$ and a high temporal cadence (12–45 s, respectively). This wide temperature coverage allows for the study of solar atmospheric structuring and dynamics from the photosphere, through the chromosphere and TR, and into the upper corona. HMI observes the 6173 Å Fe I absorption line in order to measure the Doppler shift, intensity, line-of-sight (LOS) magnetic field, and vector magnetic field of the solar photosphere. LOS magnetograms have a spatial resolution of 0.″5 and cadence of 45 s.

[5] 304 Å, $\log(T) \approx 4.7$; 131 Å, $\log(T) \approx 5.6$, 7.0; 171 Å, $\log(T) \approx 5.8$; 193 Å, $\log(T) \approx 6.2$, 7.3; 211 Å, $\log(T) \approx 6.3$; 335 Å, $\log(T) \approx 6.4$; 94 Å, $\log(T) \approx 6.8$; 1600 Å, $\log(T) \approx 5.0$; and 1700 Å, $\log(T) \approx 3.7$.

AIA data sequences of identified events are obtained through the "cutout" service at LMSAL that are of processing level 1.5 and are further corrected for solar rotation and offsets between bands (Orange et al. 2014a). HMI are precision aligned to AIA via the standard IDL procedure drot_map.pro that accounts for instrument pointing, rotation, and binning. This procedure was tested via cross-correlation of both AR and bright point coronal fields with regions of strong magnetic field polarity. Since we are considering the low-contrast QS network magnetic field, noise close to the sensitivity limit of HMI must be reduced. HMI data are processed in a custom routine that takes the average of the 3σ brightest pixels from the lowest 10% of the histogramed subregion data arrays and subtracts it from the field of view (Chesny et al. 2013).

The date, time, and location of the identified event are 2010 December 4, 11:14:24 UT, and approximate solar coordinates [−75″, 17″], respectively. Figure 1 shows the event in both wide AIA and HMI fields of view that highlight its fundamental scale difference to a typical AR. It is important to note that there are full-disk XRT data (Golub et al. 2007) from 11:05:02 to 11:12:06 UT that would be sufficient to register any X-ray brightenings from the formation of the BP. However, no X-ray signatures from this event are seen. This leads us to conclude that this event occurs at a fundamentally lower energy level than the micro-sigmoid X-ray observations of Raouafi et al. (2010).

In order to further highlight fine structure in AIA data, the wavelet transformation routine of Stenborg & Cobelli (2003) and Stenborg et al. (2008) is performed on all image sequences (Chesny et al. 2013). We use this wavelet analysis to ascertain morphological characteristics, as it provides enhanced boundaries, reduction of false event identification, and identification of previously UFS. After identification of the event, regular radiative images were used to measure event fluxes. We consider intensity enhancements in (DN/s) as defined by scaling the summation of the field-of-view flux per passband to a zero level at the beginning of the event. Observed enhancements will show a comparison of how different temperature regimes respond to the observed activity.

As we are considering observations of eruptive phenomena at a relatively high temporal cadence, the use of time–distance analyses will provide information on the velocity space over which both the plasma and magnetic dynamics occur. To accomplish these, we use a custom routine that extracts a constant user-defined row of pixels from the time series of an event and plots them sequentially. The row of pixels is chosen to lie along the path of dynamic motion so as to derive the LOS velocities.

The local magnetic field environment is a fundamental driver of solar activity. As this small-scale BP sigmoid is highly transient and shows seemingly stochastic dynamics, the fine-scale morphology of the underlying magnetic field can help determine the mechanisms behind its formation and evolution. Thus, we will consider the quantitative evolution of the local photospheric magnetic environment of this event via the evolution of the total signed magnetic flux from bipolar elements directly associated with the BP.

We also investigate quantitative modeling of these transient structures in order to help determine generation mechanisms. Determining the properties of the magnetic field above the photosphere, where flux ropes are filled with plasma, will be useful for understanding the configuration of the field where

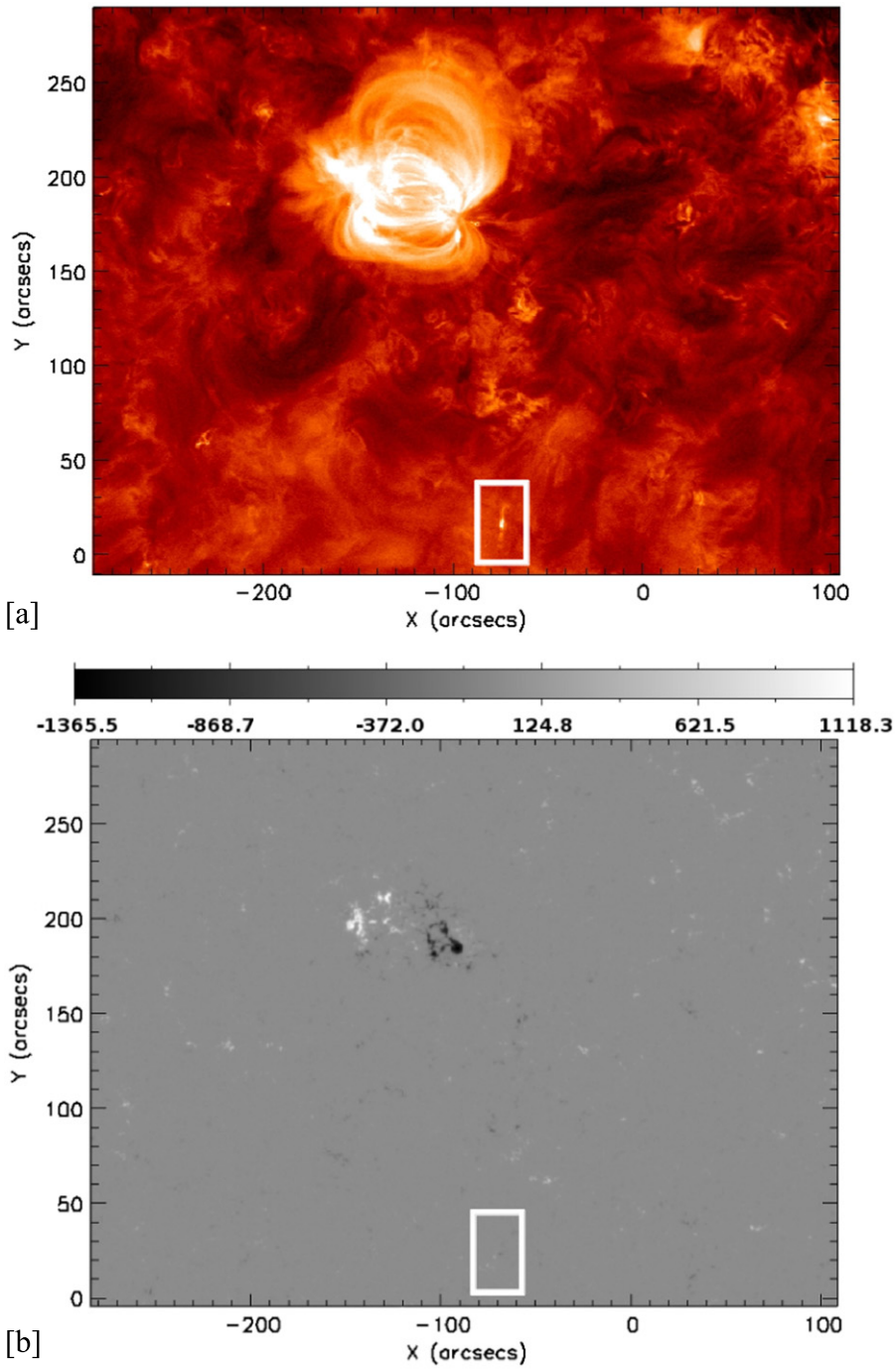

Figure 1. (a) Wide-field view of the 2010 December 4 11:14:24 UT AIA 171 Å BP sigmoid event (boxed) including active region for size comparison. (b) Wide-field view of histogramed 2010 December 4 11:14:15 UT HMI magnetogram of the BP sigmoid event (boxed). Color bar is in units of Gauss.

these structures are formed and observed. The Coronal Modeling System (CMS) software (A. A. van Ballegooijen 2011, private communication) constructs three-dimensional empirical models of the solar coronal magnetic field using photospheric magnetogram data from the HMI instrument and full-disk SOLIS Carrington rotation maps (SOLIS; Keller et al. 1998). Detailed descriptions of the model parameters and usage of the software are given by van Ballegooijen et al. (2000), Mackay & van Ballegooijen (2006), and Orange et al. (2015). CMS constructs the three-dimensional coronal magnetic field of a region of interest given an individual HMI LOS magnetogram observation. The CMS software constructs nonlinear, force-free field models and sets up the initial conditions for non-potential fields by inserting flux rope(s) into a potential field. The volume of interest is constrained by the continuous field solution between a high-resolution (HIRES) volume constrained by the supplied HMI magnetogram and the outer, low-resolution SOLIS region. The HIRES field is defined in terms of vector potentials $\boldsymbol{B} = \nabla \times \boldsymbol{A}$ so that the condition $\nabla \cdot \boldsymbol{B} = 0$ is automatically satisfied. The HIRES coronal field is calculated via variable grid spacing, which makes it possible to construct models that extend to a large height in the corona and have high spatial resolution in the lower corona and photosphere. Visualization of the computational model field are

chosen interactively via selection of footpoint regions and subsequent plotting of field line solutions. For the analyses herein, we construct CMS models for milestone morphological event times that provide sufficient photospheric relaxation times between HMI observations.

3. RESULTS

Here, we present the results of our analysis of the jet event. First, we describe the radiative morphology in the four AIA passbands of 304, 171, 193, and 211 Å (Section 3.1). Second, we examine light curve evolution of the isolated radiative emission and magnetic field strengths (Section 3.1.1). Finally, we discuss empirical measurements made with time–distance analyses and magnetic field modeling (Section 3.2).

3.1. Event Morphology

Figure 2 shows the wavelet transformed temporal evolution of the BP event in AIA 304, 171, 193, 211 Å, and HMI, top to bottom, respectively. The pre-BP configuration at 11:11 UT (first column) consists of two extended ($\gtrsim$5″) J-shaped loop features lined up end to end, separated by ∼3″, which are visually discernible above the background in all examined passbands (denoted by yellow arrows in 171 Å at 11:11:24 UT). The initial compact EUV BP occurs in between the extended loop features when the J-loops converge at 11:12 UT (second column). The peak sigmoidal form manifests at 11:14 UT (third column) as the tenuous J-loop arms emanate to the north and south from the central BP (maximum length = 14.93 ± 2.16 Mm). It is interesting to note that the footpoints of the sigmoid arms show compact brightenings in 304 Å (denoted by the green arrows at 11:14:33 UT). This sequence of converging J-loops being proceeded by chromospheric footpoint brightenings is consistent with predictions for impulsive flaring at coronal temperatures (Imada et al. 2015) and the process of tether-cutting reconnection (TCR; Moore et al. 2001; Sterling & Moore 2003; Liu et al. 2012). In the tether-cutting process, the reconnection is accompanied by high-temperature radiation. Particle acceleration along the newly reconnecting magnetic field lines would lead to the excitation of chromospheric material via thermal conduction, and this material would radiate in the EUV as footpoints of the reconnected magnetic loops (Sterling et al. 2001).

The sigmoidal configuration persists (sigmoid arcade lifetime = 03:12 ± 0:26 minutes) until each arm detaches and retreats from the central brightening (denoted by the blue arrows in 171 Å at 11:15:12 UT and visible in 193 and 211 Å), thus leaving a single BP region. The next significant morphological detail of this event is the appearance of jet eruptions that are visible in all AIA passbands (denoted by white arrows at 11:24 UT, fifth column). The eruptions show a major jet feature extending from the northwest end of the BP with a smaller jet emanating from the south (jet lifetime = 05:58 ± 0:26 minutes). This antiparallel motion is an observational analog reminiscent of bi-directional jet dynamics that are often observed in spectral data associated with BP phenomena (Doyle et al. 2004; Madjarska et al. 2004; Orange et al. 2014b). As there were no available *Hinode/EIS* data (Culhane et al. 2007; Kosugi et al. 2007) coinciding with the pointing of this event, it was not possible to observe Doppler signatures for the observed jet. However, the existence of possible bi-directional motion can have implications on the type of reconnection processes at work. The three-dimensional topology of reconnection about a magnetic NP is such that the jets follow the antiparallel one-dimensional spine axis while the loop cluster lies along the fan plane (Liu et al. 2011; Pontin et al. 2013). Further analyses in Section 4 will expand on this possible generation mechanism for the observed jet. The sideways-appearing nature of this jet is suspected to be due to the horizontal field configuration of the overlying corona. This is of the two-sided QS loop type described by Yokoyama & Shibata (1996) where the coronal field pressure inclines any open fields in the QS and make their LOS morphology to appear loop-like. This is beneficial to our on-disk observations and allows us to directly observe a QS bi-directional jet phenomenon.

3.1.1. Magnetic and Radiative Dynamics

This event lies directly along the PIL of a QS network bipole (Figure 2, HMI 11:14:15 UT contours). Figure 3 shows the zoomed-in region of the HMI box in the 11:11:15 UT frame of Figure 2. It shows a slight variation in the shape of the central negative pole over the event lifetime, and we investigate the total signed and unsigned magnetic flux of this source bipole throughout this timeframe from the boxed region at 11:11:15 UT of Figure 3. It is important to note that we chose the HMI field of view to have no loss or gain of significant flux concentrations over the considered time period. The result of this analysis is presented in Figure 4(b). Generally, the evolution of the signed magnetic flux alternates strengths throughout the event lifetime with the unsigned flux staying relatively stable, within errors. It is interesting to note that the most sigmoidal form takes place at a time where the total magnetic energy of each pole, signed and unsigned, are energetically stable. The breaking of the sigmoid occurs immediately after a rapid decrease of positive flux just before 11:15:00 UT. This is suspected to be indicative of the formation of and reconnection about a magnetic NP. This will be expanded upon in Section 3.2. The dynamic jet phenomena occur when there is a rapid increase in negative flux and simultaneous decrease in positive flux. As the total positive flux was at a peak prior to the jet initiation, we propose that the emerging negative flux reconnects continuously with the existing positive flux, thus resulting in the observed persistent jet ejection. The peak of the total signed flux occurs just prior to the jet initiation. We conjecture that this may be due to the system reaching a combined threshold of magnetic energy and kinematics that is afterward unable to confine reconnection dynamics that leads to a self-organized critical system (see Section 4).

The event light curves (Figure 4(a)) reflect a strong increase in emission in all bands corresponding with the formation of the central BP, from the chromosphere (304 Å), through the upper TR (171 Å), and into the lower (193 Å) and hot corona (211 Å). The greatest initial enhancement taking place in 304 Å could be indicative of the conduction footpoint heating resulting from TCR, as described in Section 3.1. The strongest 193 Å emission enhancement, occurring *after* the formation of the sigmoidal arcade (also consistent with TCR; Sterling et al. 2001), suggests a peak event temperature of $\gtrsim$1 MK. This empirical observation suggests that the magnetic energy levels in the QS are sufficient for inducing jet phenomena that could provide an influx of mass and energy into the corona, and perhaps the solar wind.

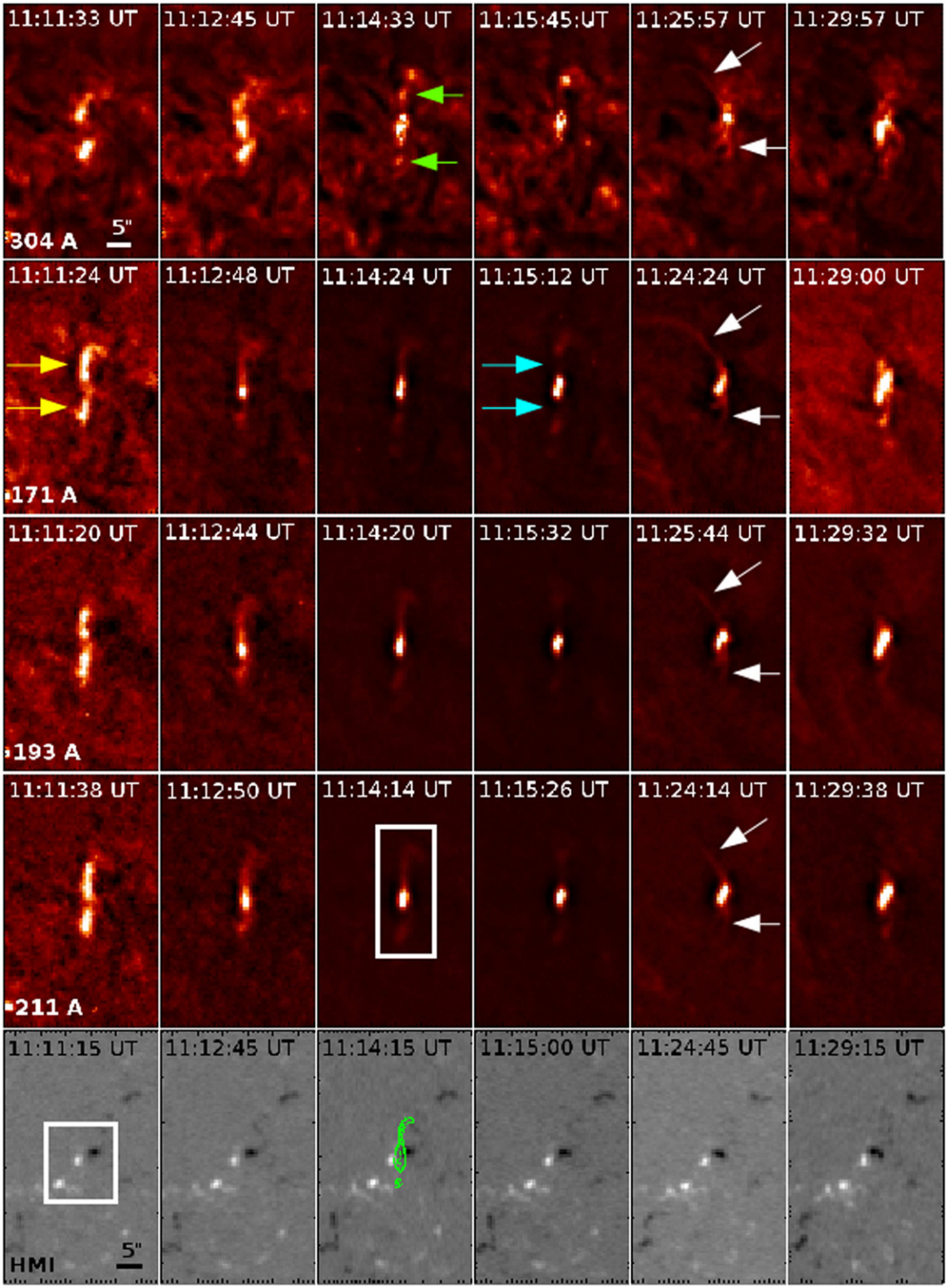

Figure 2. Wavelet transformed images of the temporal evolution of the 2010 December 4 event, in order from the top row, AIA 304, 171, 193, 211 Å, and HMI. Yellow arrows in 171 Å at 11:11:24 UT show two distinct loop structures end to end in close proximity (as also seen in 193 and 211 Å). Green arrows in 304 Å at 11:14:33 UT show compact brightenings at the loop footpoints, indicative of conduction heating due to tether-cutting reconnection. Blue arrows in 171 Å at 11:15:12 UT show the sigmoid arms being blown away from the central BP (as also seen in 193 and 211 Å). White arrows in 171 Å at 11:24:24 UT show the bi-directional jet phenomena emanating from the BP (as also seen in 193 and 211 Å). White box in 211 Å at 11:14:14 UT shows the peak sigmoidal form and the area over which light curve analyses were taken in each passband. White box in HMI at 11:14:15 UT shows the underlying magnetic field region that is considered in Figure 3. Green lines in HMI 11:14:15 UT are AIA 171 Å event contours. The BP sigmoid lies directly above a distinct QS network bipole.

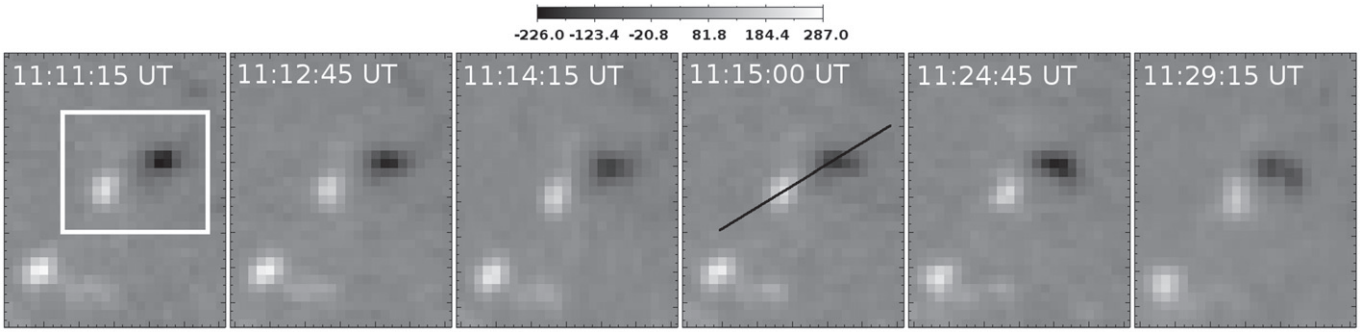

Figure 3. Zoomed-in HMI fields of Figure 2. The white box in 11:11:15 UT is the region over which the signed magnetic flux is taken. The black line crossing the bipole in 11:15:00 UT is the path extracted for time–distance analysis in Figure 5. The region was chosen so no significant flux elements enter or leave the region throughout the event sequence. Color bar units are Gauss.

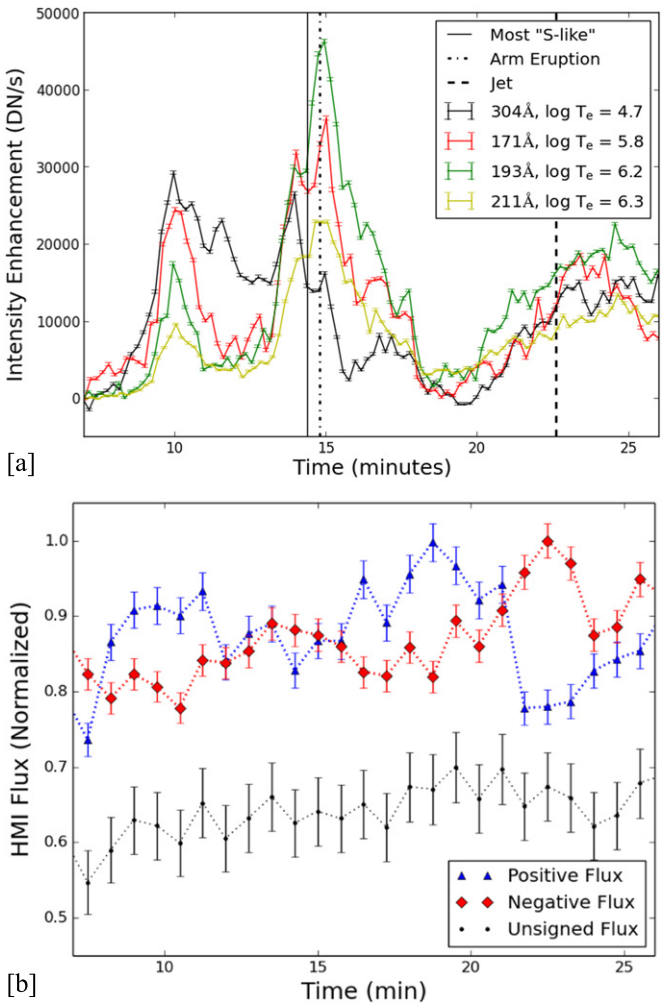

Figure 4. (a) Light curves of four AIA channels over the boxed BP mini-sigmoid region of the 211 Å 11:14:14 UT panel in Figure 2. Time is in minutes from the beginning of the hour of the event. AIA data count rates are scaled by subtracting the the data count from the first considered time, thus showing overall intensity enhancement per passband. (b) 2010 December 4 BP mini-sigmoid HMI normalized signed and unsigned magnetic flux evolution from boxed region in Figure 3. Time is in minutes from the beginning of the hour of the event. Normalized unsigned flux is scaled by −0.3 for visibility.

The fluctuations in magnetic flux observed around the time of sigmoid formation may have stressed the overlying potential field and caused it to become non-potential (Chesny et al. 2013). Such oscillatory behavior could be attributed to impulsive magnetic reconnection at an overlying magnetic NP, which is attributed with coronal BP activity (Zhang et al. 2012), and this observed configuration could be a physical manifestation of a separatrix dome (Pontin et al. 2013). This interpretation will be expanded on in the following section.

3.2. Empirical Analyses

We have conducted time–distance analyses for both AIA and HMI dynamics. For AIA, we derived the plane-of-sky velocity of the major northwest-directed jet best observed in 171 Å. The AIA jet path is shown in Figure 5(a) with the time–distance plot shown in the top panel of Figure 5(b). The jet begins its rise at 11:22:48 UT, which corresponds to 1380 s after the beginning of the 11 o'clock hour (0 s). Our best-fit line to this jet rise gives an LOS velocity of 150 ± 60 km s^{-1}. This velocity is comparable to the 80–250 km s^{-1} velocities derived for the prevalent small-scale chromospheric and TR jets observed by Tian et al. (2014) and the 160 ± 30 km s^{-1} outflow speed of polar coronal jets observed by Paraschiv et al. (2015).

Time–distance analysis of the dynamical motion of the bipole (bottom panel of Figure 5(b), with the path denoted by the black line in the 11:15:00 UT frame of Figure 3) shows the two poles migrating toward one another at a derived relative velocity of 0.96 ± 0.28 km s^{-1}. These bipole dynamics, including both convergence and signed flux variations, are indicative of self-similar processes that lead to large-scale coronal jet phenomena in stronger magnetic flux concentrations (Liu et al. 2011; Pontin et al. 2013).

We have constructed magnetic field models for milestone configurations throughout the event evolution (Figure 6) using the HMI regions of Figure 3 closest in time. At 11:11:15 UT (Figure 6(a), left panel), the modeled field lines (black) show the "J-loop" configuration as in AIA 171 Å at 11:11:24 UT (Figure 2, yellow arrows). During the peak sigmoidal form at 11:14:15 UT, CMS shows a non-potential loop with smaller underlying compact loops corresponding to the BP (Figure 6 (a), middle panel). Figure 6(b) shows the side views of the 11:14:15 UT model. These frames show the non-potential canopy overlying the central BP loop cluster. It is the magnetic bipole field oscillations of the BP that we attribute to the dynamics that induce TCR and the formation of the sigmoid. The north footpoint of the sigmoid structure is then converted into an open field configuration at 11:24:45 UT (Figure 6(a), right panel), corresponding to the time of the most extended jet

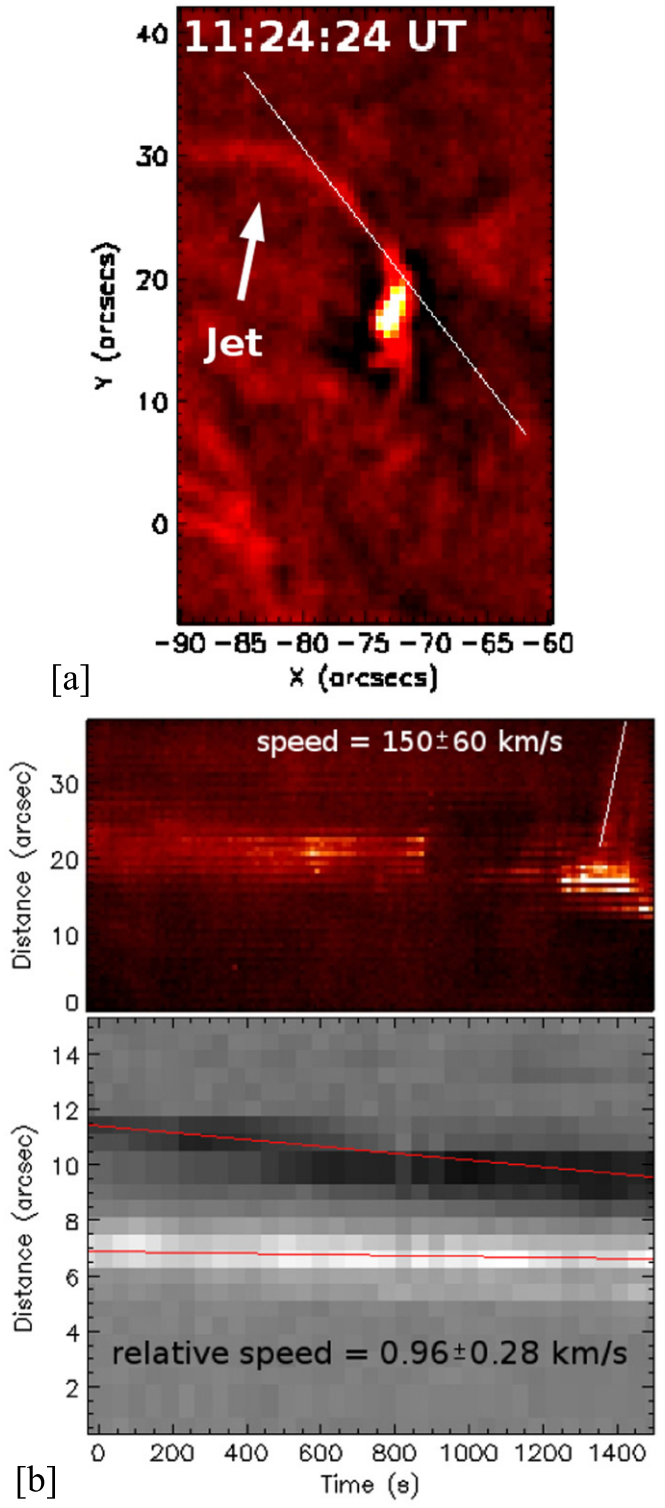

Figure 5. (a) Time–distance path of the observed jet in AIA 171 Å at 11:24:24 UT. Wavelet image is presented with increased brightness and contrast to highlight jet features. This path is taken from the sequence of images from the beginning of hour 11. (b) Time–distance plots for paths denoted in (a) (top) and HMI bipole flux convergence (bottom; from path denoted in Figure 3). The best-fit line to the AIA jet (white line) gives an LOS velocity of 150 ± 61 km s^{-1}. The best-fit lines to the HMI positive and negative pole trajectories (red lines) give a relative converging LOS velocity of 0.96 ± 0.28 km s^{-1}.

eruption. It is important to note that although the open CMS field lines eventually diverge to the east (CMS open field line solutions continue to the radial solution), they still show an initial northwestward direction (Figure 6(c)) as observed in AIA.

The modeling in Figure 6 along with the empirical measurements in Figures 4 and 5 shed light on the possible heating processes driving this unique event. The initial AIA and CMS configurations show two "J-loops" with their lower footpoints in close proximity. When there is an emergence of negative flux that can be attributed to the formation of the BP, this time-changing field may induce the tether-cutting process between these higher-lying J-loops, each with one footpoint outside the BP region, and form the non-potential arcade (Liu et al. 2010). The magnetic evolution that includes a cancelation of positive flux corresponding to the breaking of the sigmoid arms around 11:15:00 UT could be indicative of reconnection about a magnetic NP in the non-potential canopy above the BP. The formation of a NP and the resulting spine-fan topology can explain the breaking of the sigmoid and transforming the canopy (Figure 6(b)) into an open field configuration (Figure 6(c)). The continued convergence of the network bipolar field (Figure 5(b)) and a reconnecting of emerging negative flux with existing positive flux (Figure 4(b)) converts the existing magnetic energy into plasma kinetic energy. The resulting plasma outflow manifests as the observed jet following the local open magnetic field lines into the upper atmosphere.

4. DISCUSSION

Here, we have provided the first observations of EUV QS network BP activity associated with sigmoidal structuring. This BP sigmoid, as well as its eruptive nature, is the first of its kind seen to precede jet activity in such a compact, low-energy, and low-temperature environment. Our work directly addresses the question posed by Raouafi et al. (2010) as to whether there are small-scale cool BPs with sigmoidal activity, as the XRT data they used were insufficient to resolve very small BPs. Here, we show that the spatial resolution of AIA is sufficient for resolving such activity in the QS at a lower-temperature regime than X-ray observations. Going a step further, our work indicates HMI data are sufficient at resolving the QS network level magnetic fields that contribute to the formation of this previously unresolved class of structuring. This new class of structure in the low-temperature QS associating non-potential fields with jet activity is further evidence of ubiquitous magnetic reconnection throughout the solar atmosphere. The field build-up of a low-lying cluster of loops with a canopy non-potential field that leads to the opening of the above field and releasing an eruption is a strong indicator of the fan-spine reconnection topology as seen in ARs (Lynch et al. 2008; Liu et al. 2011). Although the transient behavior observed here is associated with regions of less magnetic energy (i.e., smaller) than ARs and persistent coronal BPs, our observations show that the QS network can still form and sustain BP and jet activity that reach coronal temperatures.

Magnetic field models of the identified BP sigmoid support our conclusions from AIA observations of J-loop convergence and subsequent chromospheric footpoint brightenings that the sigmoid arcade is formed via TCR. Time-varying photospheric sources can determine the behavior of the vector potential far from the individual elements. Thus, the vector potential above the photosphere can oscillate and form fields transverse to the radial distance from the source. Such dynamics may induce the TCR process at any scale in the solar atmosphere, as long as

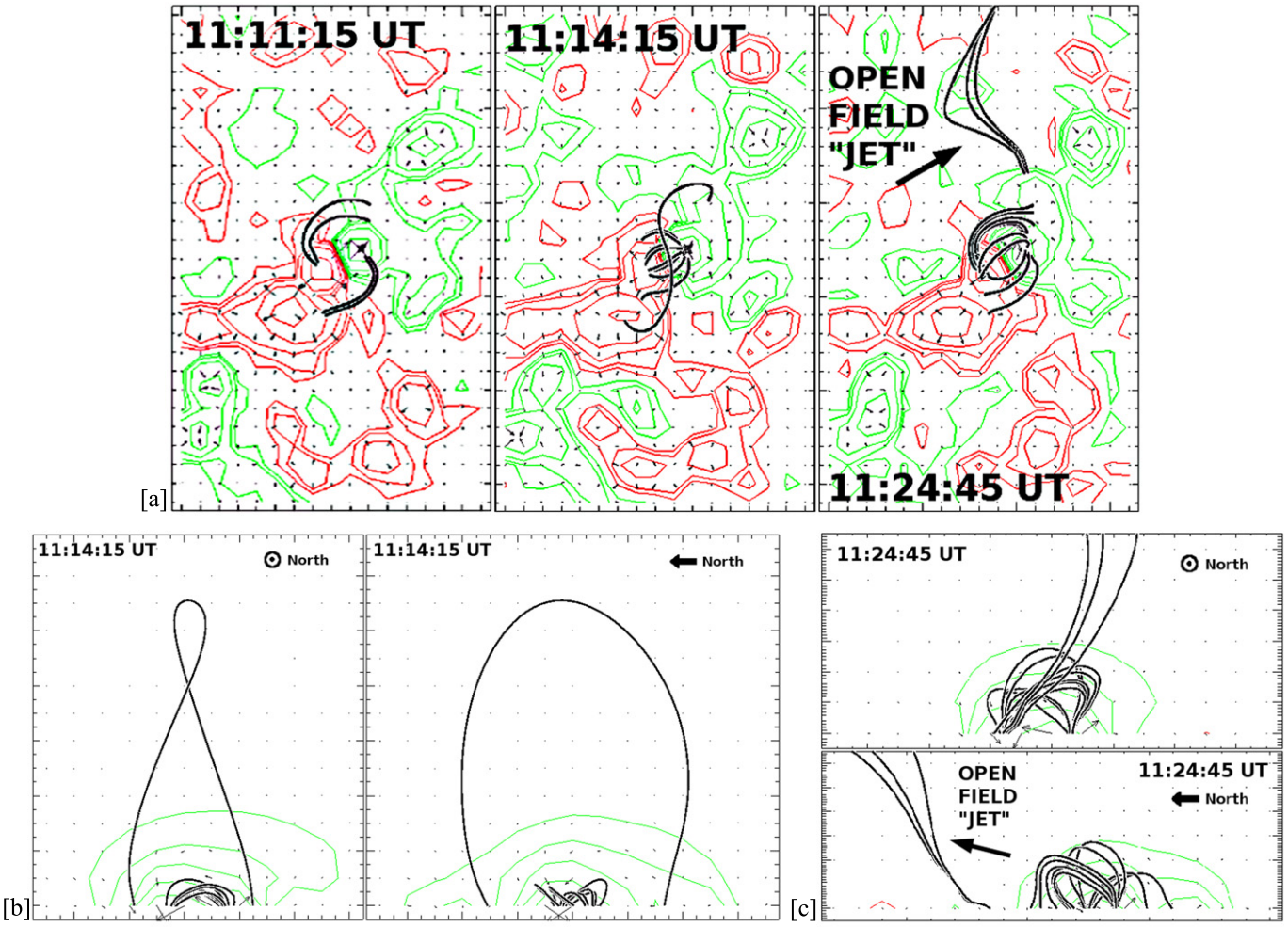

Figure 6. (a) CMS potential field models for milestone moments in the AIA evolution of Figure 2. Red (green) contours denote positive (negative) magnetic flux. Black lines are field solutions and correspond well to the observed AIA dynamics. 11:11:15 UT shows the existence of "J-shaped" loops sharing a footpoint region. 11:14:15 UT shows a low-lying cluster of compact loops with an overarching non-potential field solution akin to the observed sigmoidal AIA arcade. 11:24:45 UT shows the BP cluster with an open field region with the same trajectory to the observed jet. An unsharp mask is applied to the images for contrast. (b) Side views of the HMI 11:14:15 UT CMS model. (Left) The collection of compact loops forming the BP are seen as a low-lying cluster, with the non-potential loop solution forming the classic "tear-drop" shape viewed from the north–south direction. (Right) The non-potential loop solution forms an upper level canopy overlying the BP cluster. (c) Side views of the HMI 11:24:45 UT CMS model. (Top) The low-lying BP loop cluster is in the north–south line with the open field jet trajectory that moves off to the west. (Bottom) The west–east view shows the footpoint of the open field originating from the similar region of the north footpoint of the non-potential loop from 11:14:15 UT. It is these open field lines the jet eruption is suggested to follow.

sufficient magnetic energy is available. The resulting non-potentiality results in radiation fields, allowing for the sigmoid emission we observe. We observe time-varying photospheric magnetic energy sources leading to such activity and suggest the potential for its ubiquity throughout the QS network.

Three-dimensional models of the jet formation process above a photospheric bipole region have been shown by many authors (Török et al. 2009; Pariat et al. 2010; Masson et al. 2012) to distort canopy field lines into non-potential forms. These non-potential field lines become the separatrix field lines that contribute to the formation of a magnetic NP above the bipole, thus initiating the reconnection process that opens up the overlying field allowing for jet activity (Zhang et al. 2012). In the case of our event, we speculate that subsequent reconnection about the null breaks the sigmoid structuring and ejects each arm into an open field configuration. The morphology of the resulting jet is of a bi-directional nature inclined to the LOS as we see the main jet ejecting to the northwest and a smaller one to the south. Although we lack the spectral data that are a signature of bi-directional phenomena (Doyle et al. 2004; Madjarska et al. 2004), this uniquely observed sideways morphology, due to the downward magnetic pressure of the overlying horizontal coronal field (Yokoyama & Shibata 1996), suggests a self-similarity between other coronal bi-directional BP events (Orange et al. 2014b). In addition, this EUV QS BP sigmoid is predictive of eruptive behavior similar to soft X-ray observations of micro-sigmoids associated with vertical coronal jets (Raouafi et al. 2010) and EUV micro-sigmoids leading to micro-CMEs, further demonstrating a multi-scaled self-similarity.

As a possible global process, eruptive BP sigmoid activity is an example of self-organized criticality (SOC; Bak et al. 1987) in the QS. Reconnection dynamics leading to explosive activity can be considered as the critical point at which these systems converge (Aschwanden & Freeland 2012; Aschwanden 2014). Stresses built up in the non-potential BP field, due to the transient photospheric magnetic energy emergences and

cancelations, undergo a forced relaxation via rapid magnetic reconnection. The presented evidence of these dynamics, as well as the existence of SOC in this event, points toward solar atmospheric multi-scaled self-similarity between large-scale, high-temperature coronal fields and the small-scale, lower-temperature QS network. Similar processes manifesting at multiple scales present reconnection as ubiquitous throughout the solar atmosphere in varying plasma regimes and over varying spatial scales. QS BP sigmoid events can help constrain the power law of solar energetic events at lower temperatures than classic flare phenomena. This self-similarity between the QS and corona can also provide a lower limit to power laws of CME size and source magnetic fields.

Recently, observations from the *Interface Region Imaging Spectrograph* have associated small-scale explosive events with emerging negative polarity magnetic flux and subsequent reconnection with existing positive flux (Gupta & Tripathi 2015). Our simultaneous observations of jet activity with magnetic flux emergence, cancelation, and dynamic motions suggested by the small-scale time evolution provided by AIA and HMI suggest that such QS events may provide micro-injections of helicity into the heliosphere, a self-similar attribute to large-scale helicity injections (Raouafi et al. 2010; Wiegelmann et al. 2014; Pariat et al. 2015). That these events may provide non-negligible helicity to coronal heights and temperatures promotes the idea that QS jets cannot be ignored in the quest for a complete model of the TR. In addition, this class of network jets are necessary QS observations for constraints to a successful reconnection-driven solar wind model.

Random photospheric motions (Berger & Title 1996) coupled with the emergence and cancelation of strong magnetic flux elements (DeForest et al. 2007; Uritsky & Davila 2012) can provide suitable stressing to the localized potential magnetic field to force dynamic motions leading to TCR and non-potential fields. As we have shown, non-potential fields are non-negligible in this low-temperature QS network regime consisting of a range of network magnetic field strengths that contribute to their formation. Thus, small-scale non-potentiality should be elevated in consideration of a complete definition of the magnetic environment contributing to coronal heating and solar wind generation and may have important implications for future Sun-observing missions (Aschwanden et al. 2015).

A statistical analysis of a large ensemble of events such as the one presented here would help to elucidate their role in coronal heating contributions and may perhaps support notions to which our single-event study hints to. Furthermore, a spectral description would provide a means to investigating their LOS velocities and plasma dynamics, e.g., turbulent motions, additionally aiding such conclusions.

5. CONCLUSION

We have presented evidence of sigmoid formation associated with BP phenomena in the QS. The identification of a small-scale solar BP sigmoid has important implications for UFS in the solar atmosphere, as this previously unresolved feature class has never been associated with such small-scale QS events. The formation of non-potential fields is more ubiquitous with classes of eruptive behavior than previously thought and must be taken into more consideration for complete descriptions of the global solar magnetic field. It is evident that these stressed fields occur for numerous classes of structures, both eruptive and non-eruptive, and that they occur in small-scale QS regions exhibiting SOC. The magnetic field environment follows similar evolutions to larger-scale coronal BP counterparts and may provide micro-injections of mass, energy, and helicity to the heliosphere.

The authors thank Alphonse Sterling for useful comments and discussions. D.L.C. and N.B.O. also thank the University of the Virgin Islands. We also thank the referee for providing numerous insightful comments and literature references that greatly improved the arguments of this manuscript. N.B.O. was also supported by the Florida Space Grant Consortium, a NASA sponsored program administered by the University of Central Florida, grant NNX-10AM01H. Finally, D.L.C. and H.M.O. thank the MIT Physics department for their continued support.

REFERENCES

Aschwanden, M. J. 2014, ApJ, 782, 54
Aschwanden, M. J., & Freeland, S. L. 2012, ApJ, 754, 112
Aschwanden, M. J., Schrijver, C. J., & Malanushenko, A. 2015, arXiv:1506.04713
Bak, P., Tang, C., & Wiesenfeld, K. 1987, PhRvL, 59, 381
Berger, T. E., & Title, A. M. 1996, ApJ, 463, 365
Canfield, R. C., Hudson, H. S., & McKenzie, D. E. 1999, GeoRL, 26, 627
Chesny, D. L., Oluseyi, H. M., & Orange, N. B. 2013, ApJL, 778, L17
Culhane, J. L., Harra, L. K., James, A. M., et al. 2007, SoPh, 243, 19
DeForest, C. E., Hagenaar, H. J., Lamb, D. A., Parnell, C. E., & Welsch, B. T. 2007, ApJ, 666, 576
Doyle, J. G., Madjarska, M. S., Dzifčáková, E., & Dammasch, I. E. 2004, SoPh, 221, 51
Golub, L., Deluca, E., Austin, G., et al. 2007, SoPh, 243, 63
Gupta, G. R., & Tripathi, D. 2015, arXiv:1506.05327
Imada, S., Murakami, I., & Watanabe, T. 2015, arXiv:1506.04674
Kamio, S., Curdt, W., Teriaca, L., & Innes, D. E. 2011, A&A, 529, A21
Kankelborg, C. C., Walker, A. B. C., II, Hoover, R. B., & Barbee, T. W., Jr. 1996, ApJ, 466, 529
Keller, C. U., & the NSO staff 1998, in ASP Conf. Ser. 154, Cool Stars, Stellar Systems, and The Sun, ed. R. A. Donahue & J. A. Bookbinder (San Francisco, CA: ASP), 636
Kosugi, T., Matsuzaki, K., Sakao, T., et al. 2007, SoPh, 243, 3
Krista, L. D., Gallagher, P. T., & Bloomfield, D. S. 2011, ApJL, 731, L26
Lemen, J. R., Title, A. M., Akin, D. J., et al. 2012, SoPh, 275, 17
Liu, C., Deng, N., Liu, R., et al. 2012, ApJL, 745, L4
Liu, R., Liu, C., Wang, S., Deng, N., & Wang, H. 2010, ApJL, 725, L84
Liu, W., Berger, T. E., Title, A. M., Tarbell, T. D., & Low, B. C. 2011, ApJ, 728, 103
Longcope, D. W., Kankelborg, C. C., Nelson, J. L., & Pevtsov, A. A. 2001, ApJ, 553, 429
Lynch, B. J., Antiochos, S. K., DeVore, C. R., Luhmann, J. G., & Zurbuchen, T. H. 2008, ApJ, 683, 1192
Mackay, D. H., & van Ballegooijen, A. A. 2006, ApJ, 641, 577
Madjarska, M. S., Doyle, J. G., & van Driel-Gesztelyi, L. 2004, ApJL, 603, L57
Masson, S., Aulanier, G., Pariat, E., & Klein, K.-L. 2012, SoPh, 276, 199
McKenzie, D. E., & Canfield, R. C. 2008, A&A, 481, L65
Moore, R. L., Sterling, A. C., Hudson, H. S., & Lemen, J. R. 2001, ApJ, 552, 833
Orange, N. B., Chesny, D. L., & Oluseyi, H. M. 2015, arXiv:1501.05211
Orange, N. B., Oluseyi, H. M., Chesny, D. L., et al. 2014a, SoPh, 289, 1901
Orange, N. B., Oluseyi, H. M., Chesny, D. L., et al. 2014b, SoPh, 289, 1557
Paraschiv, A. R., Bemporad, A., & Sterling, A. C. 2015, arXiv:1505.07191
Pariat, E., Antiochos, S. K., & DeVore, C. R. 2010, ApJ, 714, 1762
Pariat, E., Dalmasse, K., DeVore, C. R., Antiochos, S. K., & Karpen, J. T. 2015, A&A, 573, A130
Pesnell, W. 2008, in COSPAR Meeting 37, 37th COSPAR Scientific Assembly, 2412
Pontin, D. I., Priest, E. R., & Galsgaard, K. 2013, ApJ, 774, 154
Raouafi, N.-E., Georgoulis, M. K., Rust, D. M., & Bernasconi, P. N. 2010, ApJ, 718, 981

Schou, J., Scherrer, P. H., Bush, R. I., et al. 2012, SoPh, 275, 229
Shibata, K., Ishido, Y., Acton, L. W., et al. 1992, PASJ, 44, L173
Shibata, K., Yokoyama, T., & Shimojo, M. 1996, AdSpR, 17, 197
Shimojo, M., Hashimoto, S., Shibata, K., et al. 1996, PASJ, 48, 123
Shimojo, M., & Shibata, K. 2000, ApJ, 542, 1100
Stenborg, G., & Cobelli, P. J. 2003, A&A, 398, 1185
Stenborg, G., Vourlidas, A., & Howard, R. A. 2008, ApJ, 674, 1201
Sterling, A. C., & Moore, R. L. 2003, ApJ, 599, 1418
Sterling, A. C., Moore, R. L., & Thompson, B. J. 2001, ApJL, 561, L219
Tian, H., DeLuca, E. E., Cranmer, S. R., et al. 2014, Sci, 346, A315
Török, T., Aulanier, G., Schmieder, B., Reeves, K. K., & Golub, L. 2009, ApJ, 704, 485
Tsuneta, S., Ichimoto, K., Katsukawa, Y., et al. 2008, SoPh, 249, 167
Uritsky, V. M., & Davila, J. M. 2012, ApJ, 748, 60
van Ballegooijen, A. A., Priest, E. R., & Mackay, D. H. 2000, ApJ, 539, 983
Wiegelmann, T., Thalmann, J. K., & Solanki, S. K. 2014, A&ARv, 22, 78
Yokoyama, T., & Shibata, K. 1996, PASJ, 48, 353
Zhang, Q. M., Chen, P. F., Guo, Y., Fang, C., & Ding, M. D. 2012, ApJ, 746, 19
Zheng, R.-S., Jiang, Y.-C., Yang, J.-Y., et al. 2013, MNRAS, 431, 1359